

Ammonia oxidizers offset acidification stress via adaptive substrate affinity in aquatic ecosystems

Received: 11 August 2025

Accepted: 14 January 2026

Published online: 27 January 2026

 Check for updatesSenwei Tong¹, Hui Shen¹, Li-Li Han², Jin-Ming Tang¹, Xianhui S. Wan¹, Zhen-Zhen Zheng²✉ & Shuh-Ji Kao²✉

Ammonia oxidation, a critical nitrogen cycle process, exhibits contradictory responses to aquatic acidification, and the underlying mechanism remains unresolved. Here, through pH manipulation experiments across diverse ecosystems and with a model ammonia-oxidizing archaea species, *Nitrosopumilus maritimus* strain SCM1, we discover a unifying adaptive mechanism: acidification triggers a compensatory increase in substrate affinity in ammonia-oxidizing microorganisms. This enhancement counteracts the reduction in ammonia availability, with the magnitude of increase being significantly greater in ammonia-oxidizing archaea than in ammonia-oxidizing bacteria. Consequently, in ammonia-oxidizing archaea-dominated systems, this adaptation can sustain or even stimulate oxidation rates under moderate acidification, while ammonia-oxidizing bacteria-dominated systems experience a decline. By incorporating this affinity response into models, we accurately reconcile prior disparate field observations. We thus establish the regulation of substrate affinity as a key determinant of microbial resilience, providing a framework for predicting nitrogen cycle dynamics under future acidification.

Aquatic systems globally—including lakes¹, estuaries^{2,3}, and the open ocean systems⁴—are undergoing rapid acidification due to rising atmospheric carbon dioxide (CO₂). Projections suggest that continued CO₂ uptake by the oceans could lower surface pH by up to 0.5 units by 2100 compared to pre-industrial levels⁵. In coastal eutrophic waters, acidification is often more pronounced, with pH declines of up to 0.85 units in oxygen-depleted subpycnocline waters due to intensified respiration⁶. Additional drivers include oxidation of reduced chemicals (e.g., ammonium, manganese(II), hydrogen sulfide, iron(II), methane), organic acid inputs, and atmospheric deposition of sulfur and nitrogen oxides^{7,8}. Understanding the impacts of acidification on biogeochemical processes is thus critical for predicting ecosystem responses to global change⁹.

Ammonia oxidation (AO), mediated by ammonia-oxidizing archaea (AOA), bacteria (AOB) and complete ammonia oxidizers (comammox), is a linchpin of the nitrogen cycle. This process initiates

the formation of nitrate (NO₃⁻), drives denitrification—a vital nitrogen loss pathway—and generates the potent greenhouse gas nitrous oxide (N₂O). While all three groups oxidize ammonia (NH₃) into nitrite (NO₂⁻), they occupy distinct niches¹⁰. Typically, AOB thrive in nutrient-rich systems (e.g., eutrophic lakes and coastal waters), whereas AOA dominate oligotrophic oceans due to their superior affinity for total ammonium (NH₃ + NH₄⁺)¹¹. In contrast, comammox *Nitrospira* species are often found in stable, low-turnover habitats such as soils, sediments, and engineered systems (e.g., biofilms and wastewater reactors)¹², and are thus expected to play a minor role in the dynamic water columns of reservoirs, estuaries, and the open ocean that are the focus of this study.

Anthropogenic nitrogen inputs and acidification are altering these dynamics¹³. Conventional models posit that pH decline reduces the availability of NH₃, which is the substrate for ammonia-oxidizing

¹State Key Laboratory of Marine Environmental Science, College of Ocean and Earth Sciences, Xiamen University, Xiamen, China. ²School of Marine Sciences, State Key Laboratory of Marine Resources Utilization in South China Sea, Hainan University, Haikou, China. ✉ e-mail: zzz@hainanu.edu.cn; sjkao@hainanu.edu.cn

microorganisms^{14–16} ($\text{NH}_3 + \text{H}^+ \rightleftharpoons \text{NH}_4^+$; $\text{p}K_a = 9.24$ at 25 °C), thereby decreasing oxidation rates^{13,17,18}. Yet, laboratory culture experiments revealed varying pH sensitivities within the same microbial lineages^{19–21}, and field studies report conflicting results, with acidification sometimes suppressing and other times enhancing rates (Supplementary Fig. 1)^{13,18,22–25}. These inconsistencies suggest NH_3 availability alone cannot explain microbial responses.

AOA's unique adaptations, such as high-affinity ammonium transporters²⁶ and acid tolerant cellular structures²⁷, may enable them to exhibit greater resilience to low pH than AOB. Yet, community-specific responses across environments remain poorly resolved, hindering predictions of nitrogen cycling under acidification.

To address these knowledge gaps surrounding acidification responses, we conducted dual-factor manipulation experiments (substrate concentration and pH) across a broad environmental gradient, from freshwater to oligotrophic oceans (Supplementary Fig. 2), and simultaneously examined the response of AOA *Nitrosopumilus maritimus* SCM1. Our results demonstrate that ammonia oxidizers can counteract acidification stress by enhancing their substrate affinity, a mechanism that reconciles previously contradictory observations. This adaptive response highlights a previously underappreciated dimension of microbial resilience, deepening our understanding of nitrogen cycle dynamics in a changing aquatic ecosystem.

Results and discussion

Diverse acidification response patterns across aquatic ecosystems

Our study captured the acidification response across a wide range of aquatic environments, from freshwater (Shanmei Reservoir, SM; $S = 0.00$) through estuarine waters (Pearl River Estuary, PRE; $S = 0.14$ – 34.30 and Jiulong River Estuary, JRE; $S = 4.10$ – 29.05), to oceanic waters (Northwest Pacific, NWP; $S = 34.84$ – 34.94). These systems exhibited contrasting nitrogen regimes: SM displayed low ammonium ($\text{NH}_4^+ = 350$ nM) but high nitrate ($\text{NO}_3^- = 131,000$ nM), reflecting efficient nitrification, while JRE showed NH_4^+ enrichment (up to 58,700 nM), indicative of anthropogenic inputs (Supplementary Table 1).

The ammonia oxidation rates (AOR) at low NH_4^+ concentration ($[\text{NH}_4^+]$ addition levels (AOR_{low} , see Methods) varied over 3 orders of magnitude, from 0.9 to 376 nM d^{-1} , across the studied environments (Fig. 1c, e, f, g, k, l). Statistical analysis revealed two primary response patterns to acidification: (I) a monotonic decline, where rates consistently declined with pH reduction (Fig. 1c); and (II) no statistically significant response, where rates remained stable or slightly increased under moderate acidification (Fig. 1e, f, g, k, l). Notably, the second pattern, with rates peaked under moderate acidification before declining, was also observed in SCM1 (Fig. 1m). The absence of significant inhibition in many field samples, coupled with the clear optimization response in SCM1, suggests a capacity for nuanced microbial adaptation to moderate acidification that counteracts a simple inhibitory effect.

The addition of high substrate concentrations partially alleviated substrate limitation and enhanced AOR in both the control and acidification treatment groups (Fig. 1a, c, e, f, g, k, m). However, interestingly, despite variations in salinity and $[\text{NH}_4^+]$ across regions, these distinct response patterns for the AOR_{low} group persisted after NH_4^+ enrichment (AOR_{high} , see Methods) (Fig. 1a–j, m), except at NWPI, where high variability obscured the trend (Fig. 1k). Critically, acidification responses were decoupled from NH_4^+ availability in multiple regions, unlike the reported dual-factor manipulation experiments revealing a $[\text{NH}_4^+]$ -dependent temperature sensitivity of AOB²⁸.

Substrate affinity as a key to modulate their acidification responses

Substrate kinetics, which include both substrate (NH_3) availability and substrate affinity, play an essential role in understanding the variable

responses of ammonia-oxidizing microorganisms to acidification. While ($\text{NH}_4^+ + \text{NH}_3$) is commonly measured and used to derive parameters for substrate kinetics in many studies^{29,30}, we specifically focus on the unionized NH_3 in our analysis (Supplementary Table 2 and 3). This is because NH_3 , as the direct substrate for AO, impacts the physiological traits of ammonia-oxidizing microorganisms and their ecological niches.

To examine these dynamics, we designed substrate kinetics experiments to assess how acidification affects the substrate affinity of ammonia-oxidizing communities (see Methods). At a given pH, we observed that oxidation rates increased with ($\text{NH}_4^+ + \text{NH}_3$) concentration ($[\text{NH}_4^+ + \text{NH}_3]$) until saturation, following either the Haldane substrate inhibition model (see Methods and Supplementary Fig. 3a) or the Michaelis–Menten model (see Methods and Supplementary Fig. 3b–g). Results from our field manipulation experiments, AOA pure culture assays, and literature-reported AOB pure cultures^{14,15,31} focused on *Nitrosomonas*, the dominant aquatic genus, show that substrate kinetic traits for ($\text{NH}_4^+ + \text{NH}_3$), including the maximum rate (V_{max}), the half saturation constant (K_m), and the substrate affinity (α), are all affected by acidification (Supplementary Table 4 and 5; Supplementary Fig. 3h–j), although no consistent trends are observed for $K_m(\text{NH}_4^+ + \text{NH}_3)$ and $\alpha(\text{NH}_4^+ + \text{NH}_3)$ under acidification (Supplementary Fig. 3i, j). While V_{max} decreases slightly with acidification ($-0.7\% \pm 0.8\%$ in field studies except at NWPI stations with high variability and $-9.0\% \pm 0.1\%$ in pure cultures per 0.1-unit pH drop; Supplementary Fig. 3h), ammonia oxidation communities are still mildly inhibited by acidification under $[\text{NH}_4^+ + \text{NH}_3]$ saturated conditions. In addition, at the SM station we observed pronounced substrate inhibition at high ammonium concentrations, which was alleviated under acidified conditions.

We specifically calculated NH_3 concentrations in each treatment group to more accurately fit the substrate kinetic model (see Methods; Supplementary Table 2 and 3). When NH_3 was used as the substrate for regression, the rates still conformed to the Haldane (Fig. 2a) or Michaelis–Menten models at a given pH (Fig. 2b–g). However, $K_m(\text{NH}_3)$ was 1 to 3 orders of magnitude lower than $K_m(\text{NH}_4^+ + \text{NH}_3)$, and $\alpha(\text{NH}_3)$ was 1 to 3 orders of magnitude higher than $\alpha(\text{NH}_4^+ + \text{NH}_3)$ (Fig. 2i, j; Supplementary Table 4 and 5; Supplementary Fig. 3i, j).

Meanwhile, both $K_m(\text{NH}_3)$ and $\alpha(\text{NH}_3)$ exhibited significant pH dependence. $K_m(\text{NH}_3)$ decreased by $-13\% \pm 8\%$ (field), $-19\% \pm 7\%$ (AOA pure culture) and $-3\% \pm 3\%$ (AOB pure culture)^{14,15,31} (Fig. 2i), whereas $\alpha(\text{NH}_3)$ increased by $28\% \pm 23\%$ (field), $94\% \pm 7\%$ (AOA pure culture) and $3 \pm 4\%$ (AOB pure culture)^{14,15,31} per 0.1-unit pH drop (Fig. 2j). This trend has also been observed in multiple pure culture studies both AOB^{15,16,20,21,31} and AOA¹⁶. These findings suggest that as acidification intensifies, ammonia-oxidizing communities require less NH_3 to maintain the same rate of activity, likely due to an improvement in their substrate utilization efficiency. Notably, in high-salinity cases (JRE1, JRE2, JRE3 and SCM1 culture), the increase in $\alpha(\text{NH}_3)$ due to acidification was significantly higher than in freshwater or low-salinity areas (SM, JRE0), as well as in AOB pure culture reported in previous studies (AOB culture) ($p < 0.05$; Fig. 2j), indicating that the acidification effect on substrate affinity was amplified for communities adapted to high salinity.

Overall, our results reveal counteractive effects of acidification on AO. Ammonia-oxidizing microorganisms enhance their substrate affinity (α towards NH_3) to accommodate acidification-induced NH_3 availability reduction. The balance between these factors likely determines the net response of AOR to acidification. Additionally, since the measured AOR reflect the activity of entire microbial communities (comprising both AOA and AOB), shifts in community composition could further influence the response of AO to acidification.

Differential Responses of AOA and AOB to Acidification

The contrasting responses of AOA and AOB to acidification provide further insights into AO dynamics. By selectively suppressing AOB activity using allylthiourea (ATU) (see Methods) and quantifying AOA/

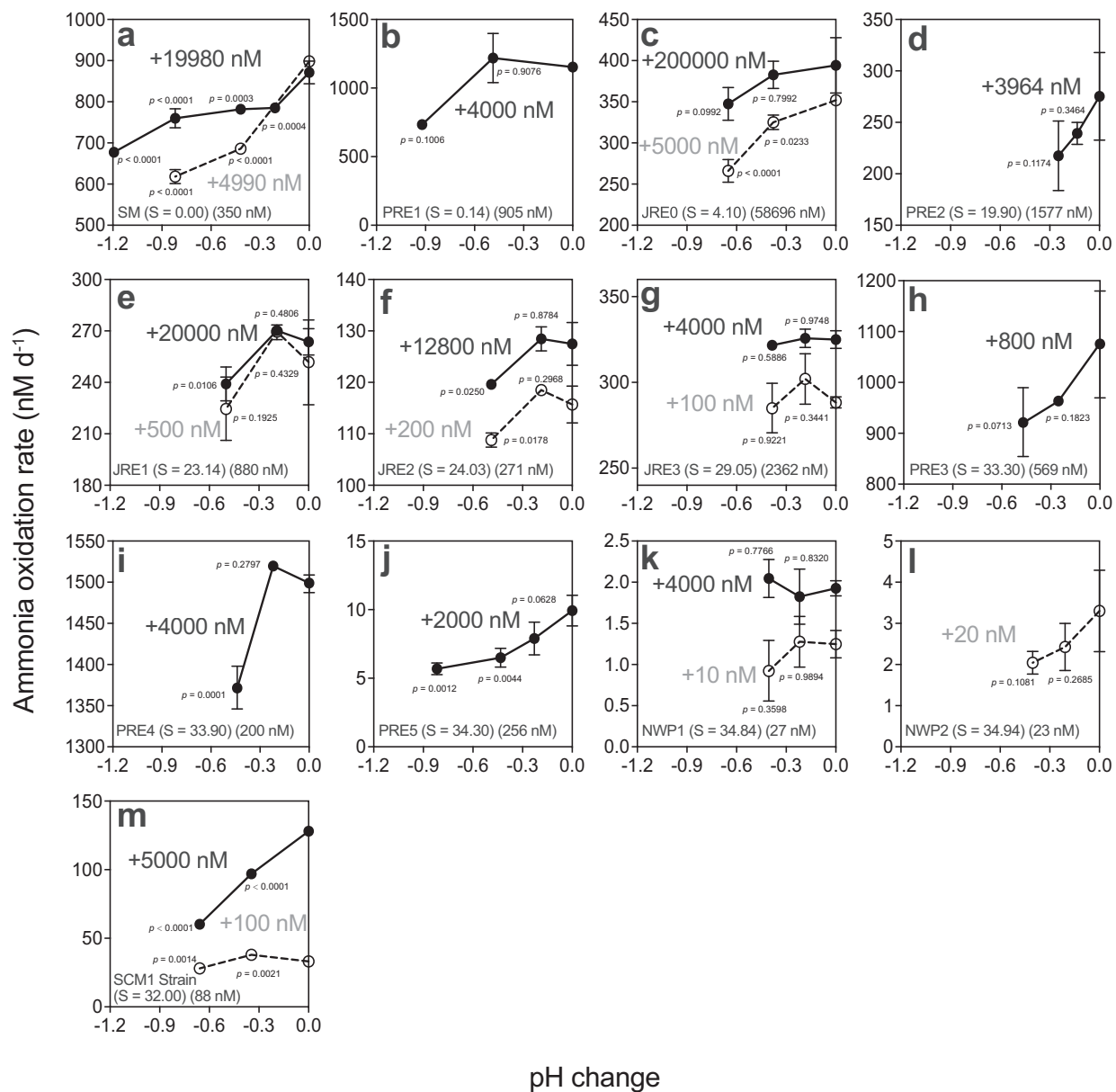


Fig. 1 | The response of ammonia oxidation rates to acidification under low and high ammonium concentration addition levels. Ammonia oxidation rates under low ammonium concentration addition levels (lower than in-situ ammonium concentration) and 4990 nM group of SM are shown as open circles with dashed lines, and the corresponding addition concentration is marked in gray next to the lines (see Methods). Ammonia oxidation rates under high ammonium concentration addition levels (higher than in-situ ammonium concentration), except 4990 nM group of SM, are shown as solid circles with solid lines and the corresponding addition concentration is marked in black next to the lines. The in-situ

salinity and ammonium concentration are labeled next to the station name. Panels (a–l) are the results of field experiments, while panel (m) is the result of pure culture of ammonia-oxidizing archaea isolate *Nitrosopumilus maritimus* SCM1. Data are presented as mean rates \pm standard deviation ($n = 3$ biologically independent samples). If error bars are not visible, they are smaller than the size of the data points. Statistical significance between treatment groups and the control group was assessed using one-way ANOVA followed by Dunnett's multiple comparisons test. Variable response patterns appear in various environments under different substrate levels.

AOB gene copy ratios (see Methods), we found that AOB dominated in freshwater and low-salinity regions (SM, PRE1 and JRE0), while AOA became predominant in higher salinity zones (Supplementary Fig. 4). This spatial shift aligned with previous estuarine observations (e.g., the Yangtze Estuary^{32,33}, the PRE^{28,33}, and the Chesapeake Bay³⁴), where AOB prefer low salinity environments and AOA dominate in higher salinities. Our kinetic analysis supports this distinction: in low-salinity areas (SM, JRE0), $K_m(\text{NH}_4^+ + \text{NH}_3)$ values exceeded 1 μM , while in high salinity regions (JRE1, JRE2, JRE3 and NWP1), $K_m(\text{NH}_4^+ + \text{NH}_3)$ values were relatively low (< 711 nM) (Supplementary Table 4).

Overall, AOA-dominated regions exhibited significantly higher AOA:AOB gene copies ratio and rate ratio relative to AOB-dominated regions ($p < 0.05$) (Fig. 3a, b). Additionally, although acidification did not cause significant differences in the V_{max} between AOB- and AOA-dominated systems (Fig. 3c), it exerted a significantly stronger effect on $K_m(\text{NH}_3)$ and $\alpha(\text{NH}_3)$ in AOA-dominated regions compared to AOB-dominated ones ($p < 0.05$) (Fig. 3d, e). This pattern was consistent with our pure culture results for SCM1 and with published data for AOB (*Nitrosomonas europaea*) (Fig. 2i, j), together suggesting that the impacts of ocean acidification on substrate affinity vary between AOB and AOA.

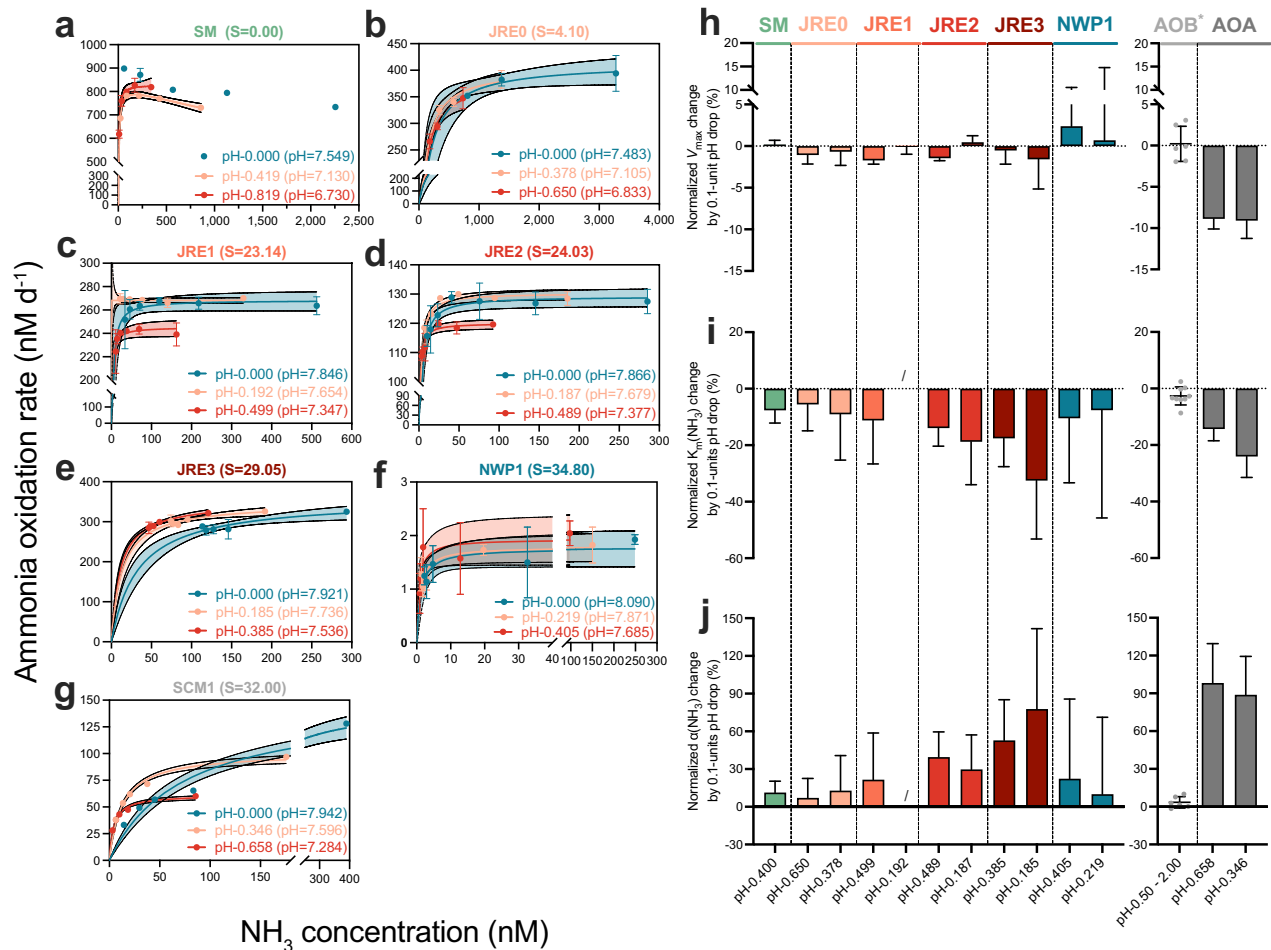


Fig. 2 | Substrate kinetic parameters towards ammonia (NH_3) at varying pH. **a–g** The dependence of ammonia oxidation rates on NH_3 concentration at varying pH. The station or strain names are labeled at the top of the graph, with the salinity values indicated next to their respective names. The legend indicates the degree of pH decrease and the pH value at this level. Solid lines in (**a–g**) represent the best fitting of Michaelis–Menten model or Haldane substrate inhibition model at various pH. The shaded area represents the 95% confidence interval. **h–j** Normalized changes in kinetic parameters towards NH_3 per 0.1-unit pH drop (V_{max} represents the maximum rate, K_m represents the half-saturation constant, and α represents the substrate affinity). Due to failure to fit the equation under in-situ pH at SM station and pH-0.192 at JRE1 station, parts of kinetic parameters are missing, and the result of pH-0.400 at the SM station is the change between two pH downregulated groups (pH-0.419 and pH-0.819). * means the data related to ammonia-oxidizing

bacteria are obtained from published studies on *Nitrosomonas europaea*, conducted under conditions with pH values ranging from 6.5 to 8.5^{14,15,31}. Data are presented as mean \pm standard deviation. Errors bars in (**a–g**) are standard deviation from triplicate incubations ($n = 3$ biologically independent samples). Data in (**h–j**) except AOB group, represent parameter estimates calculated from the fits in panels (**a–g**), error bars indicate propagated standard deviations (derived from the fit uncertainty). For AOB group in panels (**h–j**), errors bars are obtained from replicate incubations ($n = 6$ in (**h**), $n = 9$ in (**i**), and $n = 6$ in (**j**) biologically independent samples), and individual data points are shown. If error bars are not visible, they are smaller than the size of the data points. / denotes no data. At a given pH, the rates with NH_3 as the substrate follow the Michaelis–Menten model or the Haldane substrate inhibition model, and substrate kinetic parameters, including the $V_{max}(\text{NH}_3)$, $K_m(\text{NH}_3)$, and $\alpha(\text{NH}_3)$, show clear pH dependence.

To assess the individual and combined effects of acidification on substrate affinity and availability in AOA and AOB, we developed ecological models based on established substrate-level kinetics and applied them within an ecosystem context. We compared three models (see Methods): the substrate availability (S Avail) model (Fig. 4a), the substrate affinity (S Affin) model (Fig. 4b), and the combined S Avail with S Affin (S Avail + S Affin) model, incorporating both factors (Fig. 4c, d). Our findings highlight the importance of incorporating both reduced substrate availability and increased substrate affinity to accurately predict AOR under future ocean acidification scenarios, as the combined S Avail + S Affin model consistently exhibited the strongest concordance with the observation values and the lowest Root Mean Square Error (RMSE) (Supplementary Discussions; Supplementary Fig. 5,6). However, comparisons between model predictions and observed values showed marked differences in the influence of these two factors on AOR in AOA-dominated versus AOB-dominated regions (Supplementary Fig. 6, 7).

In AOB-dominated regions, RMSE of the S Avail model was smaller than that of the S Affin model (Supplementary Fig. 6a, b), indicating that the reduction in substrate availability driven by acidification was the primary driver of a sustained decline in AOR. Notably, in AOB-dominated stations, the addition of high substrate levels alleviated the negative effects of acidification (Supplementary Fig. 8a, b), but substrate availability remained the dominant limiting factor, resulting in a persistent decrease in AOR (Fig. 1a, c).

Conversely, in AOA-dominated regions and AOA pure culture experiment, the RMSE for the S Affin model was lower than that for the S Avail model, except at the NWP1 station under minor acidification (Supplementary Fig. 6c–g). This suggests that a slight pH decrease enhances substrate affinity, thereby promoting AOR (Fig. 1e, f, g, k, m). In contrast to AOB-dominated regions, the effect of substrate addition on mitigating acidification-induced changes in oxidation rates was not significant in AOA-dominated regions (Supplementary Fig. 8c–g). When substrate saturation was reached, AOR

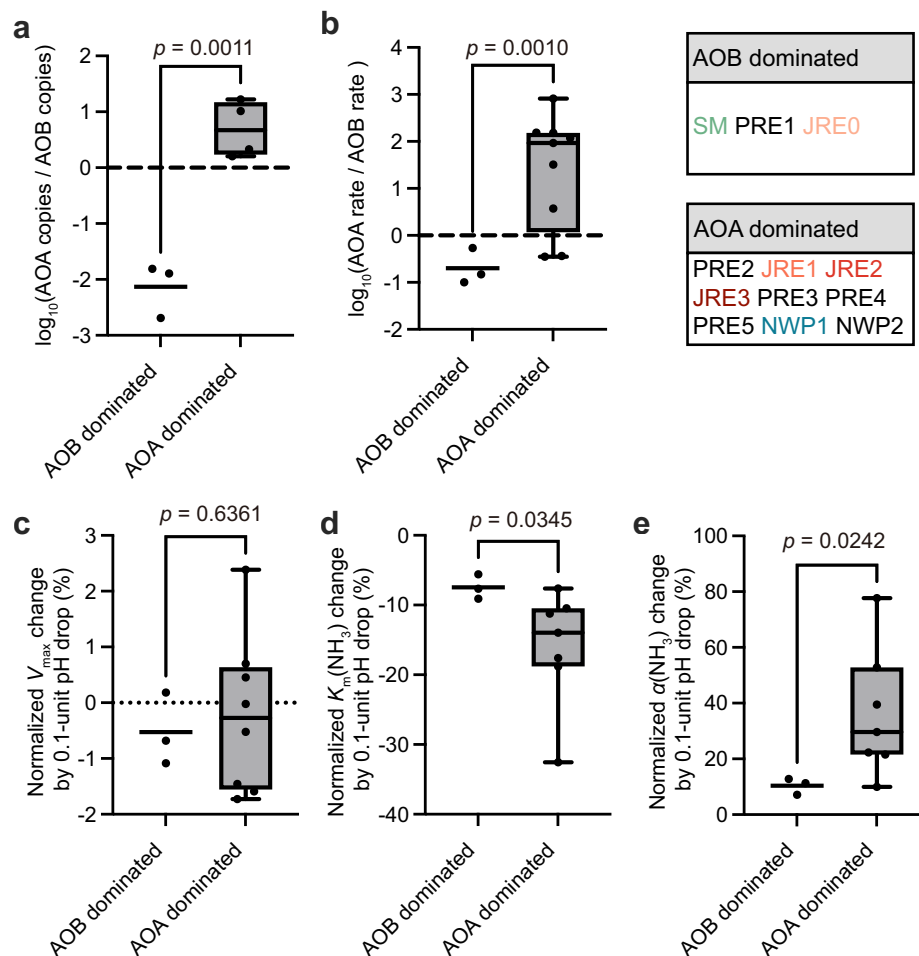


Fig. 3 | Comparative analysis of the ratio of ammonia-oxidizing archaea (AOA) to ammonia-oxidizing bacteria (AOB) contributions to rates, AOA/AOB gene copy ratios, and the impact of acidification on ammonia oxidation kinetics in AOB-dominated and AOA-dominated regions. **a** The logarithmic ratio of ammonia oxidation rates [$\log_{10}(\text{AOA rates} / \text{AOB rates})$]. **b** The logarithmic ratio of gene copies [$\log_{10}(\text{AOA copies} / \text{AOB copies})$]. **c–e** Normalized change in V_{\max} (maximum rate), K_m (half-saturation constant) and α (substrate affinity) towards NH_3 with 0.1-unit drop in pH. The stations within the AOB-dominated and AOA-dominated regions have been marked in the figure, with the stations where substrate kinetics fitting is performed

highlighted in color. Two-tailed t -test is used to examine whether there is a significant difference between AOB-dominated and AOA-dominated regions. For AOB-dominated columns, scatter dot plots with the center line depicting the mean are used ($n = 3$ biologically independent samples). For AOA-dominated columns, box-plots depict the 25–75% quantile range, with the center line representing the median (50% quantile); whiskers extend to the minimum and maximum values (**a–e**, $n = 4, 9, 8, 7$, and 7 biologically independent samples respectively). Significant differences are observed in the relative contributions of rates, gene copy numbers, and the acidification effect between AOA- and AOB-dominated regions.

were solely dependent on changes in V_{\max} , which decreased with acidification (Fig. 2h).

We extended the model to quantify the impact of changes in substrate availability and affinity on AOR under current in-situ substrate levels in both AOA- and AOB-dominated systems. In AOB-dominated regions, the ratio of the effect of increased substrate affinity to reduced substrate availability was below the $-0.5:1$ line (Fig. 4e, f). Conversely, in most AOA-dominated regions, this ratio was at or above the $-0.5:1$ line, with some regions even above the $-1:1$ line (Fig. 4e, f). This confirms that the effect of increased substrate affinity is more significant in AOA-dominated regions compared to AOB-dominated ones. These findings are consistent with results from AOB and AOA pure culture experiments (Figs. 2j and 4e). The contrasting responses between AOA- and AOB-dominated systems ($p < 0.05$) suggest that the mechanisms by which acidification affects AO differ fundamentally between the two groups.

In general, pH reduction decreases substrate availability for both AOA and AOB while increasing substrate affinity in both groups. However, at AOA-dominated sites, the increase in substrate affinity is significantly stronger than at AOB-dominated sites, and in some locations,

this effect can even outweigh the reduction in availability, which enables AOA to better adapt to acidified conditions (e.g., low concentration range in Fig. 4d). Our findings help reconcile inconsistencies in field studies on the effects of acidification on AO, where negative effects have been observed overall, but positive responses have been reported at certain AOA-dominated sites (Supplementary Fig. 1).

Potential mechanisms of ammonia-oxidizing archaea adaptation to acidification

The consistent decrease in $K_m(\text{NH}_3)$ under acidification observed in our field studies, AOA pure-culture and prior research¹⁶ confirms this is a reproducible phenotypic response across systems. This apparent enhancement in substrate affinity likely stems from a suite of physiological adjustments to low pH, rather than a direct modification of the ammonia monooxygenase (AMO) enzyme itself. As suggested by Jung et al. for other nitrifiers (*Ca. Nitrosocosmicus oleophilus* MY3 and *comammox Nitrospira inopinata*)¹⁶, factors such as shifts in cytoplasmic pH homeostasis³⁵, membrane potential²⁷, and the intracellular $\text{NH}_3/\text{NH}_4^+$ equilibrium could collectively alter substrate diffusion and uptake kinetics. Our whole-cell and community-level measurements

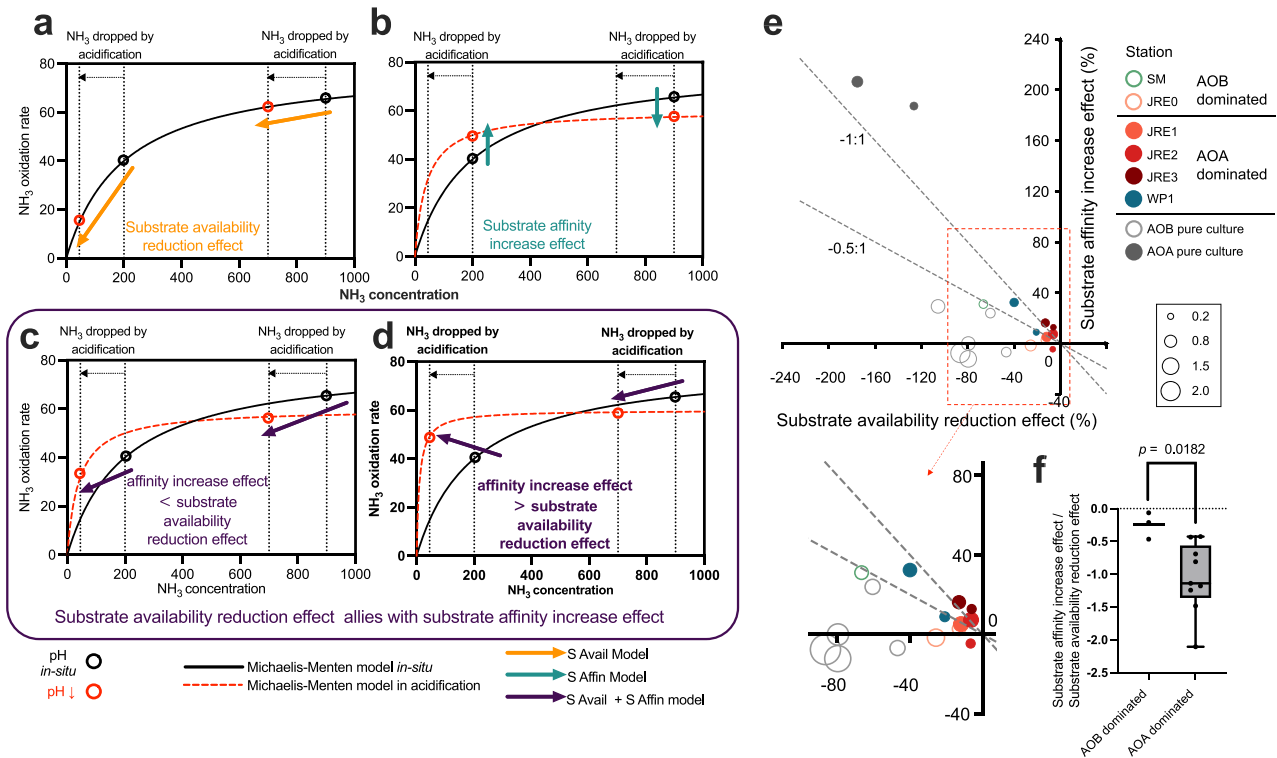


Fig. 4 | The response of the ammonia oxidation rates of two ammonia oxidizer lineages to acidification simulated by three models. a Concept model graph of substrate availability reduction effect (S Avail). **b** Substrate affinity increase effect (S Affin). **c-d** Substrate availability reduction effect combined with substrate affinity increase effect (S Avail + S Affin). **e** Relative importance of substrate availability reduction effect and substrate affinity increase effect across different stations or cultures (see Methods). **f** The ratio of the substrate affinity increase effect to the substrate availability reduction effect in ammonia-oxidizing bacteria (AOB)-dominated and ammonia-oxidizing archaea (AOA)-dominated regions. A two-tailed *t*-test

is used to examine whether there is a significant difference between AOB-dominated and AOA-dominated regions. For the AOB-dominated group, data are shown as scatter dot plots with the center line depicting the mean ($n = 3$ biologically independent samples). For the AOA-dominated group, boxplots depict the 25–75% quantile range, with the center line representing the median (50% quantile); whiskers extend to the minimum and maximum values ($n = 9$ biologically independent samples). In AOB-dominated regions, reduced substrate availability exerts a major influence, while in AOA-dominated regions, increased substrate affinity plays a more significant role.

thus reflect the integrated outcome of these complex cellular processes.

Nevertheless, substantial molecular evidence indicates that AOA are genetically equipped for a more active adaptation to acid stress. AOA express energy-dependent, high-affinity ammonium transporters^{26,36}, whereas many AOB only encode for rhesus (Rh) proteins, relying on low-affinity channels or passive diffusion^{37–39}. This fundamental difference enables AOA to scavenge and concentrate NH_3 more effectively as its external availability declines. Furthermore, AOA demonstrate a coordinated transcriptional response to acidification, including upregulation of V-ATPase to expel protons and maintain a higher intracellular pH³⁵, and increased ATP synthase expression¹⁸ to fuel this energetically costly homeostasis. The concurrent down-regulation of similar proton-pumping genes in AOB underscores a key physiological distinction between these groups.

Therefore, the enhanced substrate affinity in AOA likely arises from an intrinsic capacity to couple proton extrusion and energy generation with high-affinity transport. While acidification may not alter AMO's inherent kinetics, its overarching impact on cellular bioenergetics and membrane physiology appears to be a dominant factor shaping the observed kinetic parameters.

Ultimately, our study interprets these kinetic shifts from ecological perspectives. The mechanism of enhanced substrate utilization efficiency provides a powerful, empirically supported framework to reconcile contradictory field observations of nitrification under acidification. We posit that this adaptive response is a key determinant of microbial resilience. While the precise molecular contributors warrant further dissection via integrated transcriptomics, proteomics, and

single-cell analyses, our findings establish enhanced affinity as a critical, measurable variable for predicting nitrogen cycle dynamics in the acidifying aquatic ecosystems.

Implications for ammonia oxidation dynamics in a changing ocean

Our study reveals a critical trade-off in ammonia-oxidizing microorganisms. While acidification reduces NH_3 availability, it simultaneously enhances substrate affinity—a previously overlooked compensatory mechanism. Under the projected 0.5-unit pH decline by 2100⁵, this trade-off drives contrasting outcomes in AOB- versus AOA-dominated systems. In AOB-dominated environments (e.g., freshwater and estuaries), limited affinity gains fail to offset NH_3 scarcity (Fig. 5). This may exacerbate nitrogen accumulation, impairing eutrophication control and coastal resilience. In contrast, in AOA-dominated systems (e.g., oligotrophic ocean), high affinity adaptations ($\alpha(\text{NH}_3)$) upregulates by $36.24 \pm 22.9\%$ per 0.1-unit pH drop) sustain or even elevate oxidation rates (Fig. 5), potentially accelerating nitrogen turnover in pelagic ecosystems.

Notably, substrate-saturated conditions unmask a universal acidification stress by lowering V_{max} in both AOA- and AOB-dominated systems (Fig. 5), suggesting that even adapted communities face energetic constraints under extreme acidification. These shifts could have cumulative effects on nutrient dynamics, eutrophication potential, and overall ecosystem functioning, especially in AOB-dominated systems.

In addition, as atmospheric CO_2 concentrations increase, ocean acidification is often coupled with rising temperatures. Since warming elevates NH_3 concentrations according to the dissociation constant

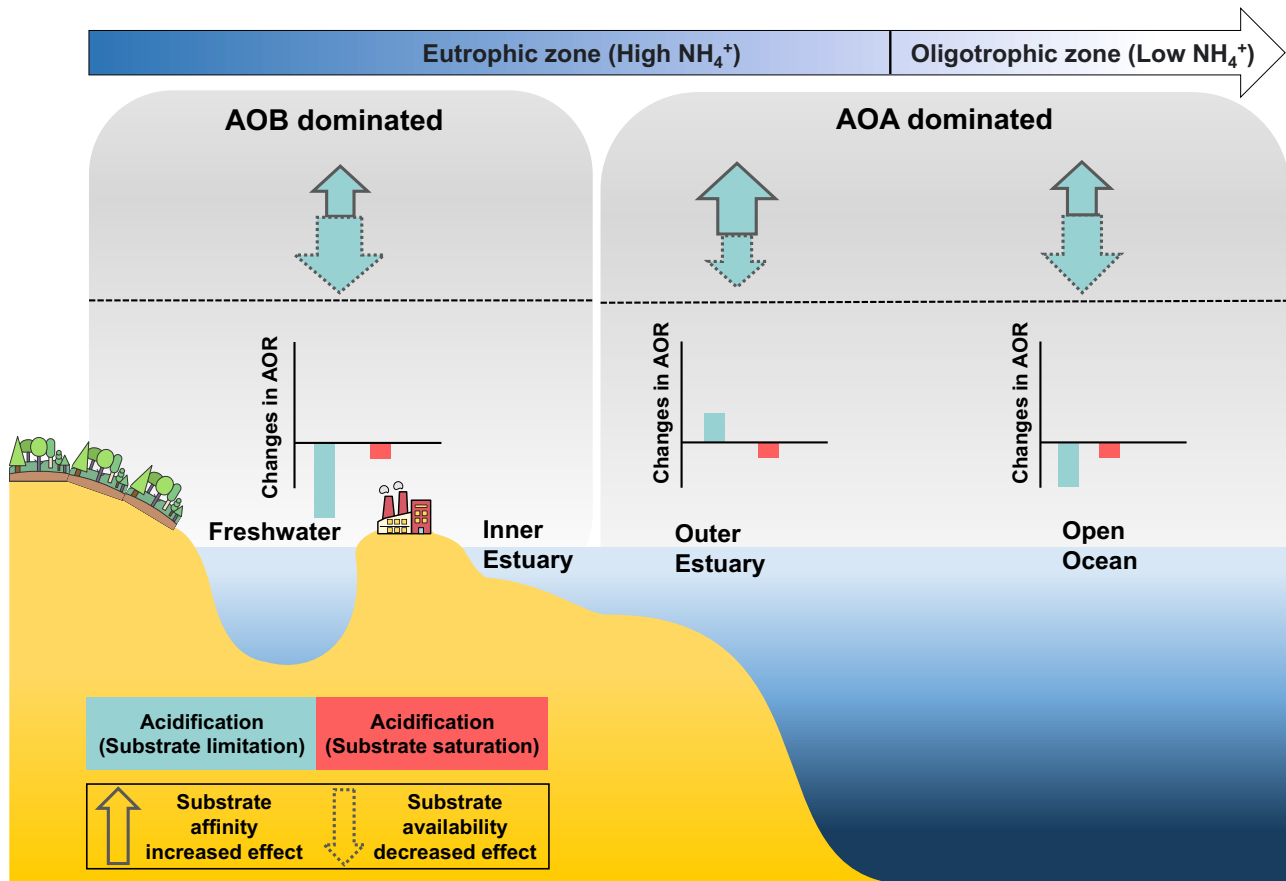


Fig. 5 | Conceptual summary of acidification effects on ammonia oxidation across different aquatic ecosystems. The diagram illustrates the shift from ammonia-oxidizing bacteria (AOB) dominance in eutrophic zones to ammonia-oxidizing archaea (AOA) dominance in oligotrophic zones. Blue bars represent ammonia oxidation rates under substrate-limited conditions, and red bars represent rates under substrate-saturated conditions. Dotted-line arrows indicate the

effect of reduced substrate availability, whereas solid-line arrows indicate the effect of increased substrate affinity. Arrow thickness reflects the relative strength of each effect. Under future scenarios of acidification, in substrate limitation conditions, ammonia oxidation rates are expected to decrease in freshwater and the open ocean but increase in the outer estuary.

calculation but reduces substrate affinity according to previous experiments²⁸ (Supplementary Fig. 9), we speculate that rising temperatures may counterbalance both the diminishing and enhancing effects of acidification on AOR. In nutrient-rich coastal regions, warming-induced NH_3 release may buffer acidification effects, but only where substrates are abundant. In contrast, in oligotrophic offshore environments where substrate availability is severely limited, warming's negative impact on affinity compounds acidification stress, potentially reducing nitrification rates by 2.2% per 0.1-unit decrease in pH, a critical feedback for oceanic N_2O emissions (See Supplementary discussions for details, Supplementary Fig. 10).

We suggest incorporating affinity-availability dynamics into earth system models to improve nitrogen cycle projections. In addition, we also highlight the need for greater focus on studies of AOA-AOB competition under multifactorial stressors (e.g., pH \times temperature \times hypoxia). By resolving the affinity-availability paradox, our work transforms the understanding of microbial resilience, offering a framework to predict nitrogen cycle disruptions in a rapidly acidifying ocean.

Methods

Field sampling

Samples were collected across six scientific expeditions spanning various trophic environments: from the eutrophic freshwater Shanmei (SM) Reservoir (January 2021), to the Pearl River Estuary (PRE) aboard the R/V Yuezhank X (July 2020 and July 2021), and the Jiulong River Estuary (JRE) aboard the R/V Ocean II (March 2023 and March 2024),

extending to the oligotrophic tropical Northwest Pacific (NWP) aboard the R/V Dongfanghong III (September–October 2021) (Supplementary Fig. 2). The specific sampling locations, including their coordinates, are shown in Supplementary Table 1 and Supplementary Fig. 2. For SM, water was gently pumped into 10 L acid-washed polycarbonate (PC) bottles using a low-pressure electric bilge pump. Temperature, salinity, and depth at SM were measured using an Idronaut Ocean Seven 316 Plus. For the PRE, NWP and JRE cruises, temperature, salinity, and depth were measured using a Seabird SBE 911 CTD sensor package, and discrete seawater samples were collected using 12- or 24-Niskin rosette systems (12 L each).

Water samples from the estuaries and reservoir were filtered through 0.2- μm syringe filters and stored in 125 mL acid-washed, seawater-rinsed, high-density polyethylene (HDPE) bottles at -20°C for subsequent nutrient analyses (NH_4^+ , NO_2^- , NO_3^-). Open ocean samples were immediately frozen at -80°C after sampling, and transferred to -20°C for storage.

Ammonia oxidation rate incubation experiments

For the ammonia oxidation rate determination, subsampled water was transferred into 120 ml glass serum bottles (CNW, Germany), pre-combusted at 450°C for 4 h, with -1 mL headspace to minimize carbonate system re-equilibration. ^{15}N -labeled NH_4Cl (98 atom% ^{15}N ; Sigma-Aldrich, 299251-1 G, Lot#TA2540V) was added to the water samples. Samples were incubated in the dark at temperatures near in-situ conditions ($\pm 2^\circ\text{C}$), with three incubation time points for most

samples, except PRE2, which had two time points. Each incubation was conducted with three replicates per treatment. At each incubation time point (including t_0), 15 mL was extracted from the serum bottles, 5 mL was for pH measurement and 10 mL was filtered through a 0.2 μm syringe filter, then stored at -20°C for subsequent NO_x^- ($\text{NO}_2^- + \text{NO}_3^-$) concentration and isotope analysis. The final concentrations of $^{15}\text{NH}_4\text{Cl}$ in the experiments and the incubation time points are presented in Supplementary Table 2 and 3.

Acidification and substrate manipulation experiments

To quantify the effect of acidification and substrate concentrations on ammonia oxidation rates, we conducted experiments manipulating pH and substrate concentrations. Because the studied environments ranged from nutrient-rich to oligotrophic zones, both in-situ $[\text{NH}_4^+ + \text{NH}_3]$ and the substrate kinetic parameters of ammonia-oxidizing microorganisms can differ substantially across sites, sometimes spanning several orders of magnitude. Accordingly, varying amounts of $^{15}\text{N-NH}_4^+$ were added to achieve a range of substrate conditions for rate measurements, and trace metal-clean HCl solutions (0.05 M or 0.1 M) were simultaneously added to adjust pH levels, prior to sealing with butyl rubber and aluminum caps (Wheaton, USA). Each station involved 3–5 pH gradients and 1–7 $^{15}\text{N-NH}_4^+$ manipulated concentrations. The specific pH values and $^{15}\text{N-NH}_4^+$ concentrations used in the experiments are listed in Supplementary Tables 2 and 3. Note that our experiments address moderate pH reductions (0.134–1.194) rather than extreme acidity. The pH of samples was measured using a pH Meter (Thermo Scientific Orion 3-Star pH Meters) equipped with a pH electrode (Thermo Scientific Orion 8102BNUWP ROSS Ultra). The pH remained very stable during the incubation (Supplementary Fig. 11).

Inhibition experiments

To differentiate the contribution of AOA and AOB to the ammonia oxidation rate, parallel incubations with $^{15}\text{NH}_4^+$ and allylthiourea (ATU) were conducted at selected stations (station SM in Shanmei Reservoir, station PRE1, PRE2, PRE3, PRE4 in the PRE in July 2020, and station JRE0, JRE2 in the JRE in March 2024). ATU was used to inhibit β -proteobacterial AOB at 80 μM ⁴⁰, allowing the measurement of AOA activity in ATU-treated samples. AOB contributions were derived by subtracting AOA rates from control (groups without ATU).

SCM1 Cultivation

Nitrosopumilus maritimus strain SCM1 was cultured in 4-(2-hydroxyethyl)-1-piperazineethanesulfonic acid (HEPES) buffered synthetic Crenarchaeota medium (SCM) at 30°C in the dark⁴¹. Cultures in the late exponential phase were transferred to fresh SCM medium (1% of inoculum) without the addition of NH_4^+ . In acidification experiments, cells were distributed into 45 centrifuge tubes with varying $^{15}\text{N-NH}_4^+$ (98% of ^{15}N atom, Sigma-Aldrich) and trace metal-clean HCl, creating substrate and pH gradients. pH was measured at each time point and each incubation vial to monitor the pH value during the incubation. Samples were filtered through 0.2 μm syringe filters, and filtrate was stored at -20°C for NH_4^+ concentration, NO_x^- concentration and NO_x^- isotope analysis.

Chemical measurements

For NH_4^+ , samples were determined within one month after sampling. At stations PRE1, PRE2, PRE3, SM, JRE0, JRE1, JRE2, and JRE3, NH_4^+ concentrations were measured using the indophenol blue spectrophotometric method with a detection limit of 0.5 μM ⁴². At station PRE4, PRE5, NWP1, NWP2, and the SCM1 culture experiment, NH_4^+ concentrations were measured using a fluorometric method with a detection limit of 0.7 nM⁴³. The concentrations of NO_2^- and NO_3^- were determined using a four-channel Continuous Flow Technicon AA3 Auto-Analyzer (Bran-Luebbe, GmbH), which has a detection limit of 30 nM for both NO_3^- and NO_2^- .

Isotopic analyses of NO_x^-

The $\delta^{15}\text{N}$ of NO_x^- was analyzed using a modified denitrifier method^{44,45}. In this method, the denitrifier strain *Pseudomonas aureofaciens* (ATCC no. 13,985) reduced NO_x^- to N_2O , subsequently the N_2O was measured using a Thermo Finnigan Gasbench system with cryogenic extraction and purification system connected to a Delta V^{PLUS} isotopic ratio mass spectrometer (GC-IRMS). The $\delta^{15}\text{N}$ of NO_x^- was calibrated by NO_3^- isotope standards USGS 34, IAEA N3 and USGS 32. The accuracy of measurements was within $\pm 0.2\text{‰}$ at an injection level of 20 nmol N and within $\pm 0.4\text{‰}$ at an injection level of 10 nmol N. For samples from station PRE5, where NO_x^- concentration was lower than 1 μM , 1 mL 1 μM NO_3^- was added as a carrier to the 9 mL samples to meet the 10 nmol N injection level requirement.

Ammonia oxidation rate calculation

The rates of ammonia oxidation were determined based on the accumulation of ^{15}N in the product pool (NO_x^-) relative to the initial pool. The rate was calculated using (Eq. 1)²⁸:

$$AOR = \frac{C_t \times n_t - C_0 \times n_0}{T \times f_{15}} \quad (1)$$

where AOR represents the ammonia oxidation rates (nM d⁻¹); C_t and C_0 are the NO_x^- concentration at the ending and beginning of the incubation (nM); n_t and n_0 are the at% ^{15}N of the NO_x^- at the ending and beginning of the incubation; T is the duration of the incubation (d); f_{15} is at% ^{15}N of the substrate pool at the beginning of the incubation.

Because the study sites span environments ranging from nutrient-rich to oligotrophic waters, both the in-situ NH_4^+ concentrations and the substrate-kinetic characteristics of ammonia-oxidizing microorganisms vary widely—often by several orders of magnitude. In general, we defined incubations with a final tracer addition of $< 1 \times$ the in-situ NH_4^+ concentration as the low- NH_4^+ treatment (AOR_{low}), whereas higher additions were classified as the high- NH_4^+ treatment (AOR_{high}). At SM station, the ambient NH_4^+ concentration was very low (~ 350 nM), yet the measured AOR was high, indicating rapid substrate turnover. To avoid rapid isotopic dilution of the added $^{15}\text{NH}_4^+$ by the ambient $^{14}\text{NH}_4^+$ pool, we applied a relatively high substrate addition (≥ 4990 nM). Consequently, both substrate-addition treatments at SM were categorized as AOR_{high}.

Fitting of substrate kinetic models

At stations SM, JRE0, JRE1, JRE2, JRE3, NWP1 and SCM1 strain incubation, we conducted substrate kinetics experiments at different pH levels to investigate the effects of acidification on the kinetic traits of ammonia oxidation communities and to more accurately evaluate the effect of acidification on AOR. For stations JRE0, JRE1, JRE2, JRE3, NWP1, and SCM1 strain incubation, we applied the Michaelis-Menten model³⁰ (Eq. 2), while at station SM, where substrate inhibition was observed, we used the Haldane substrate inhibition model³⁰ (Eq. 3) to determine the kinetic parameters.

$$AOR = \frac{V_{\max} \times S}{K_m + S} \quad (2)$$

$$AOR = \frac{V_{\max} \times S}{K_m + S + \frac{S^2}{K_i}} \quad (3)$$

where AOR is the ammonia oxidation rate, V_{\max} is the maximum reaction rate, S is the total ammonium ($\text{NH}_3 + \text{NH}_4^+$) concentration or NH_3 concentration, and K_m is the apparent half-saturation constant, representing the substrate concentration at which the reaction rate is half of V_{\max} .

K_i is the substrate concentration at which the reaction rate is reduced to half of its V_{\max} due to inhibitory effects. A nonlinear least squares regression analysis was used to estimate K_m , K_i and V_{\max} .

The substrate affinity (α) of the ammonia-oxidizing microbial community was calculated using the equation (Eq. 4):

$$\alpha = \frac{V_{\max}}{K_m} \quad (4)$$

The α values for $\text{NH}_4^+ + \text{NH}_3$ or NH_3 were calculated using the respective K_m for $\text{NH}_4^+ + \text{NH}_3$ or NH_3 .

Conversion from pH NBS scale (pH_{NBS}) to pH total scale (pH_{T})

Given the significantly higher ion strength of seawater compared to freshwater, we used AquaEnv package (an aquatic acid–base modelling environment in R) to convert the pH_{NBS} values measured by the electrode into pH_{T} ⁴⁶. This approach allowed for a more accurate evaluation of H^+ concentration in seawater.

The calculation of NH_3 concentration

NH_3 concentrations in the incubation experiments were calculated based on NH_4^+ concentrations, pH in total scale, and pK_a values using Eq. 5³:

$$\text{NH}_3 = \text{NH}_4^+ \times 10^{(\text{pH} - \text{pK}_a)} \quad (5)$$

The pK_a for each incubation experiment was calculated based on the incubation temperature and salinity⁴⁷, and summarized in Supplementary Table 2 and 3.

DNA extraction and quantitative PCR amplification

For DNA extraction, water sample was filtered through polycarbonate membranes with a pore size of 0.2 μm (25 mm in diameter; Millipore) under a pressure of < 200 mmHg (filtered volumes ranged from 0.5 to 1 L for freshwater and estuary, and 4 L for open ocean). These samples were flash frozen in liquid nitrogen and stored at -80°C until further analysis.

DNA was extracted using the DNeasy PowerSoil Pro Kit (QIAGEN, USA, CAT, 47014) following the manufacturer's instructions. The abundances of the archaeal and β -proteobacterial *amoA* gene were determined by quantitative polymerase chain reaction (q-PCR) using a CFX 96™ real-time system (BIO-RAD, Singapore). Archaeal *amoA* genes were quantified using primer set Arch-amoAF (STAATGGTCTGGCTTAGACC) and Arch-amoAR (GCGGCCATCCATCTGTATG T)⁴⁸. β -proteobacterial *amoA* genes were amplified by using primers sets amoA-1F (GGG GTTCTACTGGTGGT) and amoA-2R (CCCCTCKGSAAGCCTTCTTC)⁴⁹.

The PCR mixture was conducted following the protocol outlined by Hou et al.⁵⁰. Amplification conditions for archaeal and β -proteobacterial *amoA* genes were applied as reported by Francis et al.⁴⁸ and Rotthauwe et al.⁴⁹, respectively. The amplification products were cloned into the pMD18-T vector (TaKaRa) and then transformed into competent cells of *Escherichia coli* DH5 α . Positive clones were randomly selected for sequencing to confirm correct insertion of the target fragment. Then, equal amounts of the plasmid DNA from three different clones of the β -proteobacterial *amoA* gene and four different clones of the archaeal *amoA* gene were pooled separately to used construct standard curves for qPCR. Each standard DNA curve was serially diluted ten-fold to generate concentration ranging from 10^0 to 10^7 gene copies μL^{-1} . Standards, samples and non-template controls were amplified in triplicate with each primer set.

qPCR amplification was performed as described previously with slight modifications⁵¹. The qPCR reaction mixture (25 μL) contained 12.5 μL SYBR® Premix Ex Taq™ II (TaKaRa, Dalian, China), 5 μg Bovine Serum Albumin (BSA), 0.4 μM of each primer and 1 μL template DNA of 1–10 ng. Thermal cycling for archaeal *amoA* genes consisted of initial denaturation at 95°C for 30 s followed by 40 cycles of 95°C for 30 s, 53°C for 60 s, and 72°C for 45 s. For β -proteobacterial *amoA* gene, cycling conditions were: 94°C for 15 s, followed by 50 cycles of 94°C

for 15 s, 60°C for 30 s, and 72°C for 90 s, with a final extension of 60 s at 78°C to assure stringent product detection.

Amplification efficiencies for both archaeal and β -proteobacterial *amoA* genes ranged from 85% to 96%, with R^2 values > 0.99. The specificity of qPCR reactions was confirmed by melting curve analysis and agarose gel electrophoresis. In addition, previous studies showed that γ -proteobacterial *amoA* genes, another dominant genotype of AOB, were below the detection limit in the study area^{50,52}. Thus, γ -proteobacteria *amoA* was neglected in this analysis.

Setting of three models for ammonia oxidation response to acidification

Three theoretical models were established to evaluate the impact of substrate availability and affinity on ammonia oxidation under ocean acidification at station SM, JRE0, JRE1, JRE2, JRE3, NWPI and pure culture SCM1, with each model corresponding to a different hypothesis.

For S Avail model, we assumed that acidification only affected the concentration of substrates required by ammonia oxidizing microorganisms, that is, acidification converted a large amount of NH_3 into NH_4^+ ,

$$V_{\text{S Avail}} = \frac{V_{\max(\text{pH}_0)} \cdot S_{(\text{pH}')}(\text{NH}_3)}{k_{\text{m}(\text{pH}_0)}(\text{NH}_3) + S_{(\text{pH}')}(\text{NH}_3)} \quad (6)$$

Where $V_{\max(\text{pH}_0)}$ and $k_{\text{m}(\text{pH}_0)}(\text{NH}_3)$ were obtained from the control group fitting by Eqs. 2 and 3, $S_{(\text{pH}')}(\text{NH}_3)$ was obtained from Eq. 5 by calculating the actual concentration of NH_3 in the culture system after pH decrease.

For S Affin model, we assumed that acidification only affected the substrate affinity of ammonia oxidizing microorganisms,

$$V_{\text{S Affin}} = \frac{V_{\max(\text{pH}')} \cdot S_{(\text{pH}_0)}(\text{NH}_3)}{k_{\text{m}(\text{pH}')}(\text{NH}_3) + S_{(\text{pH}_0)}(\text{NH}_3)} \quad (7)$$

Where $V_{\max(\text{pH}')}$ and $k_{\text{m}(\text{pH}')}(\text{NH}_3)$ were obtained from the pH down-regulation group fitting by Eqs. 2 and 3, $S_{(\text{pH}_0)}(\text{NH}_3)$ was obtained from Eq. 5 by calculating the actual concentration of NH_3 in the culture system before pH decrease.

For S Avail + S Affin model, we assumed that acidification affected not only the concentration of substrates required by ammonia oxidizing microorganisms but also substrate affinity,

$$V_{\text{S Avail} + \text{S Affin}} = \frac{V_{\max(\text{pH}')} \cdot S_{(\text{pH}')}(\text{NH}_3)}{k_{\text{m}(\text{pH}')}(\text{NH}_3) + S_{(\text{pH}')}(\text{NH}_3)} \quad (8)$$

Where $V_{\max(\text{pH}')}$ and $k_{\text{m}(\text{pH}')}(\text{NH}_3)$ were obtained from the pH down-regulation group fitting by Eqs. 2 and 3, $S_{(\text{pH}')}(\text{NH}_3)$ was obtained from Eq. 5 by calculating the actual concentration of NH_3 in the culture system after pH decrease.

Evaluate the respective substrate availability decrease effect and substrate availability increase effect caused by acidification

We conducted a preliminary quantification of the intensity of the substrate availability decrease effect and substrate availability increase effect based on nutrient concentrations at various stations and three models. The actual acidification effect was calculated using the S Avail + S Affin model. The changes in the substrate affinity increase effect under acidification scenarios were determined using the S Affin model. The substrate availability decrease effect was then obtained by subtracting the effect calculated with the S Affin model from the actual acidification effect.

Temperature-pH coupled model for ammonia oxidation

The temperature-pH coupled model was designed to predict the response of ammonia oxidation rates under the framework of global change in regions dominated by different ammonia-oxidizing microorganisms (Supplementary Fig. 12). In this study, the low salinity station JRE0 was analyzed alongside the low salinity station JLR4 from Zheng et al., both of which were dominated by AOB²⁸. In contrast, the high-salinity station JRE3 was compared with the high-salinity station JI from Zheng et al., and both were identified as being dominated by AOA²⁸.

Based on the results of temperature and substrate concentration dual regulation by Zheng et al., we used the functions for $K_m(\text{NH}_4^+)$ and V_{\max} varying with temperature from their study, incorporating slight modifications to better fit our study. In brief, we used the salinity and temperature values to calculate pK_a with Eq. 5. Using the NH_4^+ concentration and the approximate pH from the study area (pH = 7.00 in JLR4 and pH = 7.90 in JI)⁵³, the concentration of NH_3 was derived. Consequently, we can fit the functions of $K_{m(T)}(\text{NH}_3)$ and $V_{\max(T)}$ with temperature (Eqs. 9 and 10)

$$K_{m(T)}(\text{NH}_3) = 2.301e^{0.174T} \quad (9)$$

$$V_{\max(T)} = 884.9e^{0.0819T} \quad (10)$$

Using the in-situ temperatures, salinity and pH data from JRE0 and JRE3, we calculate the $K_m(\text{NH}_3)$ and V_{\max} of these two stations across various temperatures and pH level (Eqs. 11 and 12), as well as the concentration of NH_3

$$K_m(\text{NH}_3) = \frac{K_{m(T)}(\text{NH}_3)}{K_{m(T)}(\text{NH}_3)} \times K'_m(\text{NH}_3) \quad (11)$$

Where $K_{m(T)}(\text{NH}_3)$ is the half-saturation constant in T (°C), $K_{m(T)}(\text{NH}_3)$ is the half-saturation constant in the same temperature as JRE0 or JRE3, $K'_m(\text{NH}_3)$ is the half-saturation constant determined in this study at the given pH,

$$V_{\max} = \frac{V_{\max(T)}}{V_{\max(T)}} \times V'_{\max} \quad (12)$$

Where $V_{\max(T)}$ is the maximum reaction rate in T (°C), $V_{\max(T)}$ is the maximum reaction rate in the same temperature as JRE0 or JRE3, V'_{\max} is the maximum reaction rate determined in this study at the given pH.

Therefore, we can compare the changes in acidification effects at different temperatures and substrate concentrations.

Statistical analyses

The comparisons between treatment groups and control groups were examined by using the Student's *t*-test. A *p*-value < 0.05 was considered statistically significant. The analyses were performed using Prism 10.

Reporting summary

Further information on research design is available in the Nature Portfolio Reporting Summary linked to this article.

Data availability

All data needed to evaluate the conclusions in the paper are deposited in Zenodo database that can be accessed through <https://doi.org/10.5281/zenodo.17795383>.

References

- Baker, L. A., Herlihy, A. T., Kaufmann, P. R. & Eilers, J. M. Acidic lakes and streams in the United States: the role of acidic deposition. *Science* **252**, 1151–1154 (1991).
- Cai, W.-J. et al. Natural and anthropogenic drivers of acidification in large estuaries. *Annu. Rev. Mar. Sci.* **13**, 23–55 (2021).
- Scanes, E., Scanes, P. R. & Ross, P. M. Climate change rapidly warms and acidifies Australian estuaries. *Nat. Commun.* **11**, 1803 (2020).
- Ma, D., Gregor, L. & Gruber, N. Four decades of trends and drivers of global surface ocean acidification. *Glob. Biogeochem. Cycles* **37**, e2023GB007765 (2023).
- Jiang, L. Q. et al. Global surface ocean acidification indicators from 1750 to 2100. *J. Adv. Model. Earth Syst.* **15**, e2022MS003563 (2023).
- Cai, W.-J. et al. Acidification of subsurface coastal waters enhanced by eutrophication. *Nat. Geosci.* **4**, 766–770 (2011).
- Cai, W. J. et al. Redox reactions and weak buffering capacity lead to acidification in the Chesapeake Bay. *Nat. Commun.* **8**, 369 (2017).
- Middelburg, J. J., Soetaert, K. & Hagens, M. Ocean alkalinity, buffering and biogeochemical processes. *Rev. Geophys.* **58**, e2019RG000681 (2020).
- Gruber, N. & Galloway, J. N. An Earth-system perspective of the global nitrogen cycle. *Nature* **451**, 293–296 (2008).
- Lehtovirta-Morley, L. E. Ammonia oxidation: Ecology, physiology, biochemistry and why they must all come together. *FEMS Microbiol. Lett.* **365**, fny058 (2018).
- Martens-Habbena, W., Berube, P. M., Urakawa, H., de la Torre, J. R. & Stahl, D. A. Ammonia oxidation kinetics determine niche separation of nitrifying Archaea and Bacteria. *Nature* **461**, 976–979 (2009).
- Koch, H., van Kessel, M. & Lucker, S. Complete nitrification: insights into the ecophysiology of comammox *Nitrospira*. *Appl. Microbiol. Biotechnol.* **103**, 177–189 (2019).
- Beman, J. M. et al. Global declines in oceanic nitrification rates as a consequence of ocean acidification. *Proc. Natl. Acad. Sci. USA* **108**, 208–213 (2011).
- Suzuki, I., Dular, U. & Kwok, S. C. Ammonia or ammonium ion as substrate for oxidation by *Nitrosomonas europaea* cells and extracts. *J. Bacteriol.* **120**, 556–558 (1974).
- Frijlink, M. J., Abee, T., Laanbroek, H. J., de Boer, W. & Konings, W. N. The bioenergetics of ammonia and hydroxylamine oxidation in *Nitrosomonas europaea* at acid and alkaline pH. *Arch. Microbiol.* **157**, 194–199 (1992).
- Jung, M. Y. et al. Ammonia-oxidizing archaea possess a wide range of cellular ammonia affinities. *ISME J.* **16**, 272–283 (2022).
- Stein, L. Y., Arp, D. J. & Hyman, M. R. Regulation of the synthesis and activity of ammonia monooxygenase in *Nitrosomonas europaea* by altering pH to affect NH_3 availability. *Appl. Environ. Microb.* **63**, 4588–4592 (1997).
- Zhou, J. et al. Effects of acidification on nitrification and associated nitrous oxide emission in estuarine and coastal waters. *Nat. Commun.* **14**, 1380 (2023).
- Qin, W. et al. Marine ammonia-oxidizing archaeal isolates display obligate mixotrophy and wide ecotypic variation. *Proc. Natl. Acad. Sci. USA* **111**, 12504–12509 (2014).
- Jones, R. D. & Morita, R. Y. Low-temperature growth and whole-cell kinetics of a marine ammonium oxidizer. *Mar. Ecol. Prog. Ser.* **21**, 239–243 (1985).
- Ward, B. B. Kinetic studies on ammonia and methane oxidation by *Nitrosococcus oceanus*. *Arch. Microbiol.* **147**, 126–133 (1987).
- Frame, C. H., Lau, E., Nolan, E. J., Goepfert, T. J. & Lehmann, M. F. Acidification enhances hybrid N_2O production associated with aquatic ammonia-oxidizing microorganisms. *Front. Microbiol.* **7**, 2104 (2016).
- Zhou, J. et al. Nitrogen input modulates the effects of coastal acidification on nitrification and associated N_2O emission. *Water Res* **261**, 122041 (2024).

24. Shiozaki, T. et al. Factors regulating nitrification in the Arctic Ocean: potential impact of sea ice reduction and ocean acidification. *Glob. Biogeochem. Cycles* **33**, 1085–1099 (2019).
25. Breider, F. et al. Response of N₂O production rate to ocean acidification in the western North Pacific. *Nat. Clim. Change* **9**, 954–958 (2019).
26. Wacker, T., Garcia-Celma, J. J., Lewe, P. & Andrade, S. L. Direct observation of electrogenic NH₄⁺ transport in ammonium transport (Amt) proteins. *Proc. Natl. Acad. Sci. USA* **111**, 9995–10000 (2014).
27. Li, P. N. et al. Nutrient transport suggests an evolutionary basis for charged archaeal surface layer proteins. *ISME J.* **12**, 2389–2402 (2018).
28. Zheng, Z. Z. et al. Substrate regulation leads to differential responses of microbial ammonia-oxidizing communities to ocean warming. *Nat. Commun.* **11**, 3511 (2020).
29. Zhang, Y. et al. Nitrifier adaptation to low energy flux controls inventory of reduced nitrogen in the dark ocean. *Proc. Natl. Acad. Sci. USA* **117**, 4823–4830 (2020).
30. Sakoula, D. et al. Enrichment and physiological characterization of a novel comammox *Nitrospira* indicates ammonium inhibition of complete nitrification. *ISME J.* **15**, 1010–1024 (2021).
31. Hunik, J. H., Meijer, H. J. G. & Tramper, J. Kinetics of *Nitrosomonas europaea* at extreme substrate, product and salt concentrations. *Appl. Microbiol. Biotechnol.* **37**, 802–807 (1992).
32. Dai, X. et al. Potential contributions of nitrifiers and denitrifiers to nitrous oxide sources and sinks in China's estuarine and coastal areas. *Biogeosciences* **19**, 3757–3773 (2022).
33. Gao, J. et al. Shifts in the community dynamics and activity of ammonia-oxidizing prokaryotes along the Yangtze estuarine salinity gradient. *J. Geophys. Res.: Biogeosci.* **123**, 3458–3469 (2018).
34. Bouskill, N. J., Eveillard, D., Chien, D., Jayakumar, A. & Ward, B. B. Environmental factors determining ammonia-oxidizing organism distribution and diversity in marine environments. *Environ. Microbiol.* **14**, 714–729 (2012).
35. Wang, B. et al. Expansion of *Thaumarchaeota* habitat range is correlated with horizontal transfer of ATPase operons. *ISME J.* **13**, 3067–3079 (2019).
36. Andrade, S. L. A., Dickmanns, A., Figner, R. & Einsle, O. Crystal structure of the archaeal ammonium transporter Amt-1 from *Archaeoglobus fulgidus*. *Proc. Natl. Acad. Sci. USA* **102**, 14994–14999 (2005).
37. Lehtovirta-Morley, L. E. et al. Identifying potential mechanisms enabling acidophily in the ammonia-oxidizing archaeon "*Candidatus Nitrosotalea devanattera*". *Appl. Environ. Microb.* **82**, 2608–2619 (2016).
38. Williamson, G. et al. A two-lane mechanism for selective biological ammonium transport. *eLife* **9**, e57183 (2020).
39. Wright, C. L. & Lehtovirta-Morley, L. E. Nitrification and beyond: metabolic versatility of ammonia oxidising archaea. *ISME J.* **17**, 1358–1368 (2023).
40. Martens-Habbena, W. et al. The production of nitric oxide by marine ammonia-oxidizing archaea and inhibition of archaeal ammonia oxidation by a nitric oxide scavenger. *Environ. Microbiol.* **17**, 2261–2274 (2015).
41. Wan, X. S. et al. Pathways of N₂O production by marine ammonia-oxidizing archaea determined from dual-isotope labeling. *Proc. Natl. Acad. Sci. USA* **120**, e2220697120 (2023).
42. Pai, S.-C., Tsau, Y.-J. & Yang, T.-I. pH and buffering capacity problems involved in the determination of ammonia in saline water using the indophenol blue spectrophotometric method. *Anal. Chim. Acta* **434**, 209–216 (2001).
43. Zhu, Y. et al. On the fluorometric measurement of ammonium in oligotrophic seawater: assessment of reagent blanks and interferences. *Limnol. Oceanogr.: Methods* **16**, 516–524 (2018).
44. Casciotti, K. L., Sigman, D. M., Hastings, M. G., Böhlke, J. K. & Hilkert, A. Measurement of the oxygen isotopic composition of nitrate in seawater and freshwater using the denitrifier method. *Anal. Chem.* **74**, 4905–4912 (2002).
45. Sigman, D. M. et al. A bacterial method for the nitrogen isotopic analysis of nitrate in seawater and freshwater. *Anal. Chem.* **73**, 4145–4153 (2001).
46. Hofmann, A. F., Soetaert, K., Middelburg, J. J. & Meysman, F. J. R. AquaEnv: an aquatic acid–base modelling environment in R. *Aquat. Geochem.* **16**, 507–546 (2010).
47. Clegg, S. L. & Whitfield, M. A chemical model of seawater including dissolved ammonia and the stoichiometric dissociation constant of ammonia in estuarine water and seawater from –2 to 40 °C. *Geochim. Cosmochim. Acta* **59**, 2403–2421 (1995).
48. Francis, C. A., Roberts, K. J., Beman, J. M., Santoro, A. E. & Oakley, B. B. Ubiquity and diversity of ammonia-oxidizing archaea in water columns and sediments of the ocean. *Proc. Natl. Acad. Sci. USA* **102**, 14683–14688 (2005).
49. Rotthauwe, J. H., Witzel, K. P. & Liesack, W. The ammonia mono-oxygenase structural gene *amoA* as a functional marker: molecular fine-scale analysis of natural ammonia-oxidizing populations. *Appl. Environ. Microb.* **63**, 4704–4712 (1997).
50. Hou, L. et al. Niche differentiation of ammonia and nitrite oxidizers along a salinity gradient from the Pearl River estuary to the South China Sea. *Biogeosciences* **15**, 5169–5187 (2018).
51. Tang, J.-M. et al. The biological transformation of ammonium and urea in a eutrophic estuarine system in Southern China. *Front. Mar. Sci.* **9**, 1040554 (2022).
52. Zheng, Z.-Z. et al. Effects of temperature and particles on nitrification in a eutrophic coastal bay in southern China. *J. Geophys. Res.: Biogeosci.* **122**, 2325–2337 (2017).
53. Roberts, E. G. et al. The carbonate system of the northern South China Sea: seasonality and exchange with the western North Pacific. *Prog. Oceanogr.* **191**, 102464 (2021).

Acknowledgements

We greatly appreciate W. Zou, E. Tan, C. Dong, L. Ge's contributions during on board sampling and incubation in the research cruises. We thank L. Tian for the help in project administration. We thank S. Li for nutrient measurements. We thank H. Wang for providing the *Nitrosopumilus maritimus* SCM1 culture. We are also grateful for Y. Lu and the crew of the R/V Ocean II, R/V Yuezhanke X, R/V Dongfanghong III for the onboard assistance and providing the CTD data. Data and samples from Pacific ocean were collected onboard R/V Dongfanghong III, implementing the NSFC open research cruise NORC2021-582. This work is supported by the National Natural Science Foundation of China (92058204, W2411034 and 42494885 to S.-J.K., 42406041 to Z.-Z.Z.). S.T. and J.-M.T. acknowledge the Ph.D. Fellowship of the State Key Laboratory of Marine Environmental Science at Xiamen University.

Author contributions

S.T., Z.-Z.Z. and S.-J.K. conceived the study and designed the experiment. S.T., H.S., L.-L.H. and J.-M.T. performed the experiments and measured the samples. S.T., L.-L.H., J.-M.T., X.S.W., Z.-Z.Z. and S.-J.K. analysed the results and structured the manuscript. All authors contributed to the discussion of the results and editing of the manuscript.

Competing interests

The authors declare no competing interests.

Additional information

Supplementary information The online version contains supplementary material available at <https://doi.org/10.1038/s41467-026-68747-z>.

Correspondence and requests for materials should be addressed to Zhen-Zhen Zheng or Shuh-Ji Kao.

Peer review information *Nature Communications* thanks the anonymous reviewers for their contribution to the peer review of this work. A peer review file is available.

Reprints and permissions information is available at <http://www.nature.com/reprints>

Publisher's note Springer Nature remains neutral with regard to jurisdictional claims in published maps and institutional affiliations.

Open Access This article is licensed under a Creative Commons Attribution-NonCommercial-NoDerivatives 4.0 International License, which permits any non-commercial use, sharing, distribution and reproduction in any medium or format, as long as you give appropriate credit to the original author(s) and the source, provide a link to the Creative Commons licence, and indicate if you modified the licensed material. You do not have permission under this licence to share adapted material derived from this article or parts of it. The images or other third party material in this article are included in the article's Creative Commons licence, unless indicated otherwise in a credit line to the material. If material is not included in the article's Creative Commons licence and your intended use is not permitted by statutory regulation or exceeds the permitted use, you will need to obtain permission directly from the copyright holder. To view a copy of this licence, visit <http://creativecommons.org/licenses/by-nc-nd/4.0/>.

© The Author(s) 2026